

# Ozone enhancement due to photo-disassocation of nitrous acid in eastern China

Xuexi Tie<sup>1,2</sup>, Xin Long<sup>1,5</sup>, Guohui Li<sup>1</sup>, Shuyu Zhao<sup>1</sup>, Jianming Xu<sup>3,4</sup>

<sup>1</sup>KLACP, SKLLQG, Institute of Earth Environment, Chinese Academy of Sciences, Xi'an 710061, China

<sup>2</sup>Center for Excellence in Urban Atmospheric Environment, Institute of Urban Environment, Chinese Academy of Sciences, Xiamen 361021, China

<sup>3</sup> Shanghai Meteorological Service, Shanghai, 200030, China

<sup>4</sup>Shanghai Key Laboratory of Meteorology and Health, Shanghai, 200030, China

<sup>5</sup>School of Environment Science and Engineering, Southern University of Science and Technology, Shenzhen 518055, China

*Correspondence to:* XueXi Tie ([tiexx@ieecas.cn](mailto:tiexx@ieecas.cn)) or  
Jianming Xu ([metxuim@163.cn](mailto:metxuim@163.cn))

28 **Abstract**

29  $\text{PM}_{2.5}$ , a particulate matter with a diameter of 2.5 micrometers or less, is one of the  
30 major components of the air pollution in eastern China. In the past few years, China's  
31 government made strong efforts to reduce the  $\text{PM}_{2.5}$  pollutions. However, another  
32 important pollutant (ozone) becomes an important problem in eastern China. Ozone  
33 ( $\text{O}_3$ ) is produced by photochemistry, which requires solar radiation for the formation  
34 of  $\text{O}_3$ . Under heavy  $\text{PM}_{2.5}$  pollution, the solar radiation is often depressed, and the  
35 photochemical production of  $\text{O}_3$  is prohibited. This study shows that during fall in  
36 eastern China, under heavy  $\text{PM}_{2.5}$  pollutions, there were often strong  $\text{O}_3$   
37 photochemical productions, causing a co-occurrence of high  $\text{PM}_{2.5}$  and  $\text{O}_3$   
38 concentrations. This co-occurrence of high  $\text{PM}_{2.5}$  and  $\text{O}_3$  is un-usual and is the main  
39 focus of this study. Recent measurements show that there were often high HONO  
40 surface concentrations in major Chinese mega cities, especially during daytime, with  
41 maximum concentrations ranging from 0.5 to 2 ppbv. It is also interesting to note that  
42 the high HONO concentrations were occurred during high aerosol concentration  
43 periods, suggesting that there were additional HONO surface sources in eastern China.  
44 Under the high daytime HONO concentrations, HONO can be photo-dissociated to be  
45 OH radicals, which enhance the photochemical production of  $\text{O}_3$ . In order to study the  
46 above scientific issues, a radiative transfer model (TUV; Tropospheric  
47 Ultraviolet-Visible) is used in this study, and a chemical steady state model is  
48 established to calculate OH radical concentrations. The calculations show that by  
49 including the OH production of the photo-dissociated of HONO, the calculated OH  
50 concentrations are significantly higher than the values without including this  
51 production. For example, by including HONO production, the maximum of OH  
52 concentration under the high aerosol condition (AOD=2.5) is similar to the value  
53 under low aerosol condition (AOD=0.25) in the no-HONO case. This result suggests  
54 that even under the high aerosol condition, the chemical oxidizing process for  $\text{O}_3$   
55 production can occurred, which explain the co-occurrence of high  $\text{PM}_{2.5}$  and high  $\text{O}_3$   
56 in spring and fall seasons in eastern China. However, the  $\text{O}_3$  concentrations were not  
57 significantly affected by the appearance of HONO in winter. This study shows that  
58 the seasonal variation of solar radiation plays important roles for controlling the OH  
59 production in winter. Because the solar radiation is in a very low level in winter,  
60 adding the photolysis of HONO has smaller effect in winter than in fall, and OH

61 remains low values by including the HONO production term. This study provides  
62 some important scientific highlights to better understand the O<sub>3</sub> pollutions in eastern  
63 China.

64

65 **Keywords; High PM<sub>2.5</sub> and O<sub>3</sub>, eastern China, HONO photolysis**

66

67

68

69

70

71

72 **1. Introduction**

73

74 Currently, China is undergoing a rapid economic development, resulting in a higher  
75 demand for energy and greater use of fossil fuels. As a result, the high emissions of  
76 pollutants produce heavy pollutions in mega cities of eastern China, such as Beijing  
77 and Shanghai. For example, in the city of Shanghai (a largest mega city in China), the  
78 urban and economical developments of the city are very rapid. During 1990 to 2015,  
79 the population increased from 13.3 to 24.1 million. The number of automobiles  
80 increased from 0.2 million (1993) to 2.0 million (2011). The rapid growing population  
81 and energy usage caused a rapid increase in the emissions of pollutants, leading to  
82 severe air pollution problems in these mega cities (Zhang et al., 2006; Geng et al.,  
83 2007; Deng et al., 2008).

84

85 Measurements, such as satellite observations have revealed much higher aerosol  
86 pollution in eastern China than in eastern US (Tie et al., 2006). The high aerosol  
87 pollution causes a wide range of environmental consequences. According to a study  
88 by Tie et al. (2009a), exposure to extremely high particle concentrations leads to a  
89 great increase of lung cancer cases. High PM (particular matter) concentrations also  
90 significantly reduce the range of visibility in China's mega cities (Deng et al., 2008).  
91 According to a recent study, the high aerosol pollution causes important effects on the  
92 crop (rice and wheat) production in eastern China (Tie et al., 2016).

93

94 In the troposphere, ozone formation is resulted from a complicated chemical process,  
95 and requires ozone precursors, such as VOCs (volatile organic carbons) and NO<sub>x</sub> =  
96 NO + NO<sub>2</sub> (nitrogen oxides) (Sillman, 1995). As the increase in industrial activity and  
97 number of automobiles, the precursors of ozone (O<sub>3</sub>) and the global budget of  
98 oxidization are also significantly increased (Huang et al., 2017; Huang et al., 2018).  
99 As a result, O<sub>3</sub> pollutions are becomes a serous pollution problem in Shanghai and  
100 other Chinese mega cities (Geng et al., 2010; Tie 2009b; Tie et al., 2015). The effects  
101 on O<sub>3</sub> production rate can be characterized as either NO<sub>x</sub>-sensitive or VOC-sensitive  
102 conditions (Sillman, 1995; Zhang et al., 2003; Lei et al., 2004; Tie et al., 2013). Thus,  
103 better understanding the trends of O<sub>3</sub> precursors (VOCs, NO<sub>x</sub>) is important to  
104 determine the O<sub>3</sub> trends in Shanghai (as well as many large cities in China).

105 In the past few years, China's government made strong efforts to reduce the PM<sub>2.5</sub>  
106 pollutions. However, another important pollutant (O<sub>3</sub>) becomes an important problem  
107 in eastern China. Several studies regarding the O<sub>3</sub> formation are previously studied in  
108 Shanghai. For example, Geng et al. (2007; 2008) study the relationship between O<sub>3</sub>  
109 precursors (NOx and VOCs) for the ozone formation in Shanghai. Tie et al. (2009)  
110 study the short-term variability of O<sub>3</sub> in Shanghai. Their study suggested that in  
111 addition to the ozone precursors, meteorological conditions, such as regional transport,  
112 have also strong impacts on the ozone concentrations. During September 2009, a  
113 major field experiment (the MIRAGE-Shanghai) was conducted in Shanghai, and  
114 multiply chemical species were measured during the experiment. The summary of the  
115 measurements by Tie et al (2013) suggests that the ozone formation in Shanghai is  
116 under VOC-sensitive condition. However, if the emission ration of NOx/VOCs  
117 reduces to a lower value (0.1-0.2), the ozone formation in Shanghai will switch from  
118 VOC-sensitive condition to NOx-sensitive condition.

119 Despite of some progresses have been made for the ozone formation in mega cities in  
120 China, it is still lack of study of ozone development in large cities of China. For  
121 example, this study shows that during fall in eastern China, under heavy PM<sub>2.5</sub>  
122 pollutions, there were often strong O<sub>3</sub> chemical productions, causing the  
123 co-occurrence of high PM<sub>2.5</sub> and O<sub>3</sub> concentrations. Under heavy aerosol condition,  
124 the solar radiation is depressed, significantly reducing the photochemical production  
125 of O<sub>3</sub>. This co-occurrence of high PM<sub>2.5</sub> and O<sub>3</sub> is an unusual and is the focus of this  
126 study. He and Carmichael (1999) suggest that aerosol particles can enhance the  
127 scattering of solar radiation, enhancing the flux density inside the boundary layer.  
128 Recent measurements also show that there were often high HONO concentrations in  
129 major Chinese mega cities, especially during daytime, with maximum concentrations  
130 ranging from 0.5 to 2 ppbv (Huang et al., 2017). Shi et al. (2015) suggest that there  
131 are several potential HONO sources, including surface emissions, conversion of NO<sub>2</sub>  
132 at the ocean surface, etc., and adding these sources can improve the calculated HONO  
133 concentrations. It is also interesting to note that the high HONO surface  
134 concentrations were occurred during high aerosol concentration periods, suggesting  
135 that there are additional HONO surface sources in eastern China. Under the high  
136 daytime HONO concentrations, HONO can be photo-dissociated to be OH radicals,  
137 which enhance the photochemical production of O<sub>3</sub>.

139 The paper is organized as follows: in Section 2, we describe the measurement of O<sub>3</sub>  
140 and PM<sub>2.5</sub>. In Section 3, we describe the calculation of photo-dissociated rate of  
141 HONO and a steady state model for the calculation of OH, and the causes of high O<sub>3</sub>  
142 production under the heavy aerosol condition. Section 4 shows a brief conclusion of  
143 the results.

## 145 **2. Measurements of O<sub>3</sub> and PM<sub>2.5</sub>**

147 There are long-term measurements in Eastern China by Chinese Environment  
148 Protection Agency (CEPA) for monitoring the air quality in China. In eastern China,  
149 especially in the capital city of China (Beijing), there are often heavy air pollutions,  
150 especially for fine particular matter (PM<sub>2.5</sub> – the radius of particle being less than 2.5  
151 um). Figure 1 shows the measurement sites in Beijing, in which the measured  
152 concentrations of PM<sub>2.5</sub> and O<sub>3</sub> are used to the analysis. In the region, the air  
153 pollutions were very heavy, especially in winter (Long et al., 2016; Tie et al., 2017).  
154 The previous studies suggested that the both aerosol and O<sub>3</sub> pollutions became the  
155 major pollutants in the region (Li et al., 2017).

157 Figure 2 shows the daily averaged concentrations of PM<sub>2.5</sub> and O<sub>3</sub> in the Beijing  
158 region in 2015. The daily averaged concentrations show that there were strong daily  
159 and seasonal variations for both the concentrations of PM<sub>2.5</sub> and O<sub>3</sub>. Despite the daily  
160 variation, the concentrations of PM<sub>2.5</sub> existed a strong seasonal variation. For example,  
161 there were very high concentrations during winter, with maximum of ~300  $\mu\text{g}/\text{m}^3$ .  
162 While in summer, the maximum concentrations reduced to ~150  $\mu\text{g}/\text{m}^3$ . The seasonal  
163 variability of O<sub>3</sub> concentrations were opposite with the PM<sub>2.5</sub> concentrations, with  
164 lower concentrations in winter (< 50  $\mu\text{g}/\text{m}^3$ ) and higher concentrations in summer (>  
165 150  $\mu\text{g}/\text{m}^3$ ). These seasonal variations of PM<sub>2.5</sub> and O<sub>3</sub> have been studied by previous  
166 studies (Tie and Cao, 2017; Li et al., 2017). Their results suggest that the winter high  
167 PM<sub>2.5</sub> concentrations were resulted from the combination of both the high emissions  
168 (heating season in the Beijing region), and poor meteorological ventilation conditions,  
169 such as lower PBL (Planetary Boundary Layer) height (Quan et al., 2013; Tie et al.  
170 2015). According to the photochemical theory of O<sub>3</sub> formation, the summer high and

171 winter low O<sub>3</sub> concentrations are mainly due to seasonal variation of the solar  
172 radiation (Seinfeld, J. H. and Pandis, 2006).

173

174 In addition to the seasonal variation of solar radiation, the heavy aerosol  
175 concentrations play important roles to reduce solar radiation, causing the reduction of  
176 solar radiation and O<sub>3</sub> formation (Bian et al., 2007). As we show in Fig. 3a, during  
177 wintertime, the O<sub>3</sub> concentrations were strong anti-correlated with the PM<sub>2.5</sub>  
178 concentrations, suggesting that the reduction of solar radiation by aerosol particles  
179 have important impact on the reduction of O<sub>3</sub> concentrations. Figure 3a also shows  
180 that the relationship between O<sub>3</sub> and PM<sub>2.5</sub> was not linearly related. For example,  
181 when the concentrations of PM<sub>2.5</sub> were less than 100  $\mu\text{g}/\text{m}^3$ , O<sub>3</sub> concentrations rapidly  
182 decreased with the increase of PM<sub>2.5</sub> concentrations. In contrast, when the  
183 concentrations of PM<sub>2.5</sub> were greater than 100  $\mu\text{g}/\text{m}^3$ , O<sub>3</sub> concentrations slowly  
184 decreased with the increase of PM<sub>2.5</sub> concentrations. This is consistent with the result  
185 of Bian et al (2007).

186

187 It is interesting to note that during late spring, summer, and early fall periods, the  
188 correlation between PM<sub>2.5</sub> and O<sub>3</sub> concentrations was positive relationship compared  
189 to the negative relationship in winter (see Fig. 3b). This result suggests that O<sub>3</sub>  
190 production was high during the heavy haze period, despite the solar radiation was  
191 greatly depressed. In order to clearly display this unusual event, we illustrate diurnal  
192 variations of PM<sub>2.5</sub> and O<sub>3</sub>, and NO<sub>2</sub> during a fall period (from Oct.5 to Oc. 6, 2015).  
193 Figure 4 shows that during this period (as a case study), the PM<sub>2.5</sub> concentrations were  
194 very high, ranging from 150 to 320  $\mu\text{g}/\text{m}^3$ . Under such high aerosol condition, the  
195 solar radiation should be significantly reduced, and O<sub>3</sub> photochemical production  
196 would be reduced. However, the diurnal variation of O<sub>3</sub> was unexpectedly strong,  
197 with high noontime concentration of  $>220 \mu\text{g}/\text{m}^3$  and very low nighttime  
198 concentration of  $\sim 25 \mu\text{g}/\text{m}^3$ . This strong diurnal variation was due to the  
199 photochemical activity, which suggested that during relatively low solar conditions,  
200 the photochemical activities of O<sub>3</sub> production was high. According to the theory of the  
201 O<sub>3</sub> chemical production, the high O<sub>3</sub> production is related to high oxidant of OH  
202 (Seinfeld and Pandis, 2006), which should not be occurred during lower solar  
203 radiation. This result brings important issue for air pollution control strategy, because  
204 the both air pollutants (high PM<sub>2.5</sub> and O<sub>3</sub>) were important air pollution problems in

205 eastern China.

206

207 To clearly understand the effect of the high aerosol concentrations on solar radiation,  
208 we investigate the meteorological conditions, such as cloud covers, relation humidity  
209 (RH), and solar radiation during the period of the case study (see Figs. 5 and 6).  
210 Figure 5 shows that the cloud condition was close to the cloud free condition, but  
211 there was a very heavy aerosol layer in the Beijing region, suggesting that cloud cover  
212 played a minor role in the reduction of the solar radiation. The measured RH values  
213 (not shown) were generally higher than 60%, with a maximum of 95% during the  
214 period. As a result, the high aerosol concentrations companied by high RH produced  
215 important effects on solar radiation. As shown in Fig. 6, the daytime averaged solar  
216 radiation was significantly reduced (about 40% reduction in Oct. 5-6 period compared  
217 with the value of Oct. 8).

218

## 219 **2. Method**

220

221 In order to better understand the  $O_3$  chemical production occurred in heavy aerosol  
222 condition in eastern China, the possible  $O_3$  production in such condition is discussed.  
223 Ozone photochemical production ( $P[O_3]$ ) is strongly related to the amount of OH  
224 radicals (Chameides et al., 1999). According to the traditional theory, the amount of  
225 surface OH radicals is proportional to the surface of solar radiation, which is  
226 represented by

227

$$228 [OH] = P[HOx]/L[HOx]^* \quad (R-1)$$

229

230 Where  $[OH]$  represents the concentration of hydroxyl radicals ( $\#/cm^3$ );  $HOx$   
231 represents the concentration of  $HO_2 + OH$  ( $\#/cm^3$ );  $P[HOx]$  represents the  
232 photochemical production of  $HOx$  ( $\#/cm^3/s$ ); and  $L[HOx]^*$  (1/s) represents the  
233 photochemical destruction of  $HOx$ , which is normalized by the concentrations of OH.

234

235 The major process for the photochemical production of  $P[HOx]$  is through the  $O_3$   
236 photolysis and follows by the reaction with atmospheric water vapor. It can express  
237 by

$$238 P[HOx] = J_1[O_3]/(k_1 \times am) \times 2.0 \times k_2[H_2O] = P_1[HOx] \quad (R-2)$$

239 Where  $J_1$  represents the photolysis of  $O_3 + h\nu \rightarrow O^1D$ ;  $k_1$  represents the reaction rate  
240 of  $O^1D + am \rightarrow O^3P$ ; and  $k_2$  represents the reaction rate of  $O^1D + H_2O \rightarrow 2OH$ . As  
241 we can see, this HOx production is proportional to the magnitude of solar radiation  
242 ( $J_1$ ), and  $J_1$  is the  $O_3$  photolysis with the solar radiation. Figure 7 shows the  
243 relationship between the values of  $J_1$  and aerosol concentrations in October at  
244 middle-latitude calculated by the TUV model (Madronich and Flocke, 1999). This  
245 result suggests that under the high aerosol concentrations (AOD = 2.5), the  $J_1$  value is  
246 strongly depressed, resulting in significant reduction of OH concentrations and  $O_3$   
247 production. For example, the maximum  $J_1$  value is about  $2.7 \times 10^{-5}$  (1/s) with lower  
248 aerosol values (AOD = 0.25). According to the previous study, the surface  $PM_{2.5}$   
249 concentrations were generally smaller than  $50 \mu\text{g}/\text{m}^3$  with this AOD value (Tie et al.,  
250 2017). However, when the AOD value increase to 2.5 (the  $PM_{2.5}$  concentrations are  
251 generally  $>100 \mu\text{g}/\text{m}^3$ ), the maximum  $J_1$  value rapidly decreases to about  $6 \times 10^{-6}$  (1/s),  
252 which is about 450% reduction compared to the value with AOD=0.25. This study  
253 suggests that under high  $PM_{2.5}$  concentrations ( $>100 \mu\text{g}/\text{m}^3$ ), the photochemical  
254 production of OH (P[HOx]) is rapidly decreased, leading to low OH concentrations,  
255 which cannot initiate the high oxidation of  $O_3$  production. As a result, the high  $O_3$   
256 production shown in Fig. 4 cannot be explained. Other sources for  $O_3$  oxidation are  
257 needed to explain this result.

259  
260 Recent studies show that the HONO concentrations are high in eastern China (Huang  
261 et al., 2017). Because under high solar radiation, the photolysis rate of HONO is very  
262 high, resulting in very low HONO concentrations in daytime (Seinfeld and Pandis,  
263 2006). These measured high HONO concentrations are explained by their studies.  
264 One of the explanations is that there are high surface HONO sources during daytime,  
265 which produces high HONO concentrations (Huang et al., 2017). Shi et al. (2015)  
266 suggest that there are several potential HONO sources, including surface emissions,  
267 conversion of  $NO_2$  at the ocean surface, etc. Zhang et al. (2016) parameterized these  
268 potential HONO sources in the WRF-Chem model, and the calculated HONO  
269 concentrations are increased in the WRF-Chem model. In our calculation, we only use  
270 the classical gas-phase chemistry to calculate HONO concentrations, and to illustrate  
271 that the importance of these missing sources for the production of OH radicals.

272 Adding these missing sources (there are not fully understand and remain a large  
273 uncertainty) could be a very important future work.

274

275 Figure 8 shows the measured HONO concentrations in three large cities in China  
276 (Shanghai, Xi'an, and Beijing) during fall and winter. It shows that the measured  
277 HONO concentrations were high, with a maximum concentration of 2.3 ppbv during  
278 morning, and about 0.5-1.0 ppbv in daytime. As a result, we think that the high  
279 HONO is a common event in large cities in eastern China, especially in daytime. This  
280 high HONO is also measured by previous studies (Zhang et al. 2016; Huang et al.  
281 2017). In this study, we make an assumption that the co-occurrence between O<sub>3</sub> and  
282 PM<sub>2.5</sub> occurred under high HONO concentrations. We note that using this assumption  
283 may result in some uncertainties in estimating the effect of HONO on OH. For  
284 example, using the measured HONO in Xi'an and Beijing could produce 1-2 times  
285 higher OH production by photolysis of HONO than the result by using the data from  
286 Shanghai. In this case, we use the measured HONO from Shanghai to avoid the over  
287 estimate of the HONO effect, which can be considered as a low-limit estimation.

288

289 It is also interesting to note that the high HONO concentrations were occurred during  
290 high aerosol concentration periods. Figure 9 illustrates that when the PM<sub>2.5</sub>  
291 concentrations increased to 70-80  $\mu\text{g}/\text{m}^3$ , and the HONO concentrations enhanced to  
292 1.4-18 ppbv during September in Shanghai. This measured high HONO  
293 concentrations were significantly higher than the calculated concentrations (shown in  
294 Fig. 8), suggesting that some additional sources of HONO are needed. This result is  
295 consistent with the HONO measurements in other Chinese cities (Huang et al. 2017).

296

297 Under the high HONO concentrations in daytime, HONO can be photolyzed to be OH,  
298 and become another important process to produce OH. As a result, the OH production  
299 rate (P[HO<sub>x</sub>]) can be written to the following reactions.

300

$$301 \quad P_2[\text{HO}_x] = J_2 \times [\text{HONO}] \quad (\text{R-3})$$

$$302 \quad P[\text{HO}_x] = P_1[\text{HO}_x] + P_2[\text{HO}_x] \\ 303 \quad = J_1[\text{O}_3]/(k_1 \times \text{am}) \times 2.0 \times k_2[\text{H}_2\text{O}] + J_2 \times [\text{HONO}] \quad (\text{R-4})$$

304

305 Because the chemical lifetime of OH is less than second, OH concentrations can be  
306 calculated according to equilibrium of chemical production and chemical loss. With  
307 the both OH chemical production processes, the OH concentrations can be calculated  
308 by the following equation (Seinfeld and Pandis, 2006).

309

310 
$$P1 + P2 = L1 + L2$$

311

312 Where  $P1$  and  $P2$  are the major chemical productions, expressed in R-4, and  $L1$  and  
313  $L2$  are the major chemical loss of OH, and represent by

314



317

318 Under high NO<sub>x</sub> condition, such as in the Shanghai region, NO<sub>x</sub> concentrations were  
319 often higher to 50 ppbv (shown in Fig. 3), the  $L1$  term is larger than  $L2$ . The OH  
320 concentrations can be approximately expressed by

321

322 
$$[HO] = \{J_1[O_3]/(k_1 \times am) \times 2.0 \times k_2[H_2O] + J_2 \times [HONO]\}/$$
  
323  $k_3[NO_2] \quad (R-5)$

324

325 Where  $k_3$  is the reaction coefficient of  $OH + NO_2 \rightarrow HNO_3$ .

326

### 327 **3. Result and analysis**

#### 328 **3.1. OH productions in different HONO conditions**

329

330 In order to quantify the individual effects of these two OH production terms ( $P1$  and  
331  $P2$ ) on the OH concentrations, the  $P1$  and  $P2$  are calculated under different daytime  
332 HONO conditions (calculated low HONO and measured high HONO concentrations).  
333 Figure 10 shows that under the low HONO condition, the  $P1$  is significantly higher  
334 than  $P2$ , and  $P2$  has only minor contribution to the OH values. For example, the  
335 maximum of  $P1$  occurred at 13 pm, with a value of  $65 \times 10^6 \text{#/cm}^3/\text{s}$ . In contrast, the  
336 maximum of  $P2$  occurred at 10 am, with a value of  $15 \times 10^6 \text{#/cm}^3/\text{s}$ . However, under  
337 high HONO condition, the  $P2$  plays very important roles for the OH production. The  
338

339 maximum of P1 occurred at 11 am, with a value of  $350 \times 10^6 \text{#/cm}^3/\text{s}$ , which is about  
340 500% higher than the P1 value. It is important to note that this calculation is based on  
341 the high aerosol condition (AOD = 2.5) in September. This result can explain the high  
342 O<sub>3</sub> chemical production in Fig. 4.

343

### 344 **3.2. OH in different aerosol conditions**

345

346 In order to understand the effect of aerosol conditions, especially high aerosol  
347 conditions, on the OH concentrations. Figure 11 shows the OH concentrations with  
348 and without HONO production of OH. With including the HONO production (i.e.,  
349 including P1 and P2), the calculated OH concentrations are significantly higher than  
350 without including this production (i.e., only including P1). The both calculated OH  
351 concentrations are rapidly changed with different levels of aerosol conditions. For  
352 example, without HONO production, the maximum OH concentration is about  
353  $7.5 \times 10^5 \text{#/cm}^3$  under low aerosol condition (AOD=0.25). In contrast, the maximum  
354 OH concentration rapidly reduced to  $1.5 \times 10^5 \text{#/cm}^3$  under high aerosol condition  
355 (AOD=2.5), and further decreased to  $1.0 \times 10^5 \text{#/cm}^3$  with the AOD value of 3.5. In  
356 contrast, with including HONO production, the OH concentrations significantly  
357 increased. Under higher aerosol condition (AOD=2.5), the maximum of OH  
358 concentration is about  $7.5 \times 10^5 \text{#/cm}^3$ , which is the same value under low aerosol  
359 condition in the no-HONO case. This result suggests that the measured high O<sub>3</sub>  
360 production occurred in the high aerosol condition is likely due to the high HONO  
361 concentrations in Shanghai.

362

### 363 **3.3. Effects of clouds**

364

365 Cloud cover can have very important impacts on the photolysis of HONO, which can  
366 affect the effect of HONO on the OH radicals. The above calculations are based on  
367 the cloud-free condition, with heavy aerosol concentration in the Beijing region. As  
368 shown in Fig. 5, during the case study period (Oct 5 to 6, 2015) (see Fig. 4), the  
369 weather map shows that the cloud-free condition, with heavy aerosol condition.

370

371 In order to understand the effects of cloud on the photolysis of HONO, we include  
372 different cloud covers in the TUV model. The calculated results show in Fig. 12.  
373 The results show that the thin cloud (with cloud cover in 2 km and cloud water of 10

374 g/m<sup>3</sup>), could reduce the photolysis rate of HONO by about 40%, but the HONO could  
375 still remain important effects. However, with dense cloud condition (with cloud  
376 covers at 2 and 3 km and cloud water of 50 10 g/m<sup>3</sup>), the photolysis rate of HONO  
377 could reduce by 9-10 times by the cloud. In this case, adding photolysis rate of  
378 HONO cannot produce important effect on OH radicals and the production of O<sub>3</sub>.

379

### 380 **3.3. OH in winter**

381

382 The measurement of O<sub>3</sub> also shows that the concentrations in winter were always low  
383 (see Fig. 2), suggesting that the O<sub>3</sub> concentrations were not significantly affected by  
384 the appearance of HONO. Figure 10 shows the OH concentrations in September and  
385 December. It shows that under different aerosol conditions, OH concentrations in  
386 December were very low compared with the values in September. Both the calculated  
387 OH concentrations include the HONO production term. For example, under the  
388 condition of AOD=2.5, the maximum OH is about  $7.5 \times 10^5$  #/cm<sup>3</sup> in September, while  
389 it rapidly reduces to  $1.5 \times 10^5$  #/cm<sup>3</sup> in December. Under the condition of AOD=3.5,  
390 the maximum OH is still maintaining to a relative high level ( $4.5 \times 10^5$  #/cm<sup>3</sup>) in  
391 September. However, the maximum OH values are extremely low in December, with  
392 maximum value of  $0.5 \times 10^5$  #/cm<sup>3</sup> in December. Because both the OH chemical  
393 productions (P1 and P2) are strongly dependent upon solar radiation (see equation  
394 R-4), the seasonal variation of solar radiation plays important roles for controlling the  
395 OH production in winter (see Fig. 13). Because the solar radiation is in a very low  
396 level in winter, adding the photolysis of HONO has smaller effect in winter than in  
397 fall, and OH remains low values by including the HONO production term.

398

## 399 **Summary**

400

401 Currently, China is undergoing a rapid economic development, resulting in a high  
402 demand for energy, greater use of fossil fuels. As a result, the high emissions of  
403 pollutants produce heavy aerosol pollutions (PM<sub>2.5</sub>) in eastern China, such as in the  
404 mega city of Beijing. The long-term measurements show that in addition to the heavy  
405 aerosol pollution, the O<sub>3</sub> pollution becomes another major pollutants in the Beijing  
406 region. The measured results show that there were very strong seasonal variation in  
407 the concentrations of both PM<sub>2.5</sub> and O<sub>3</sub> in the region. During winter, the seasonal  
408 variability of O<sub>3</sub> concentrations were anti-correlated with the PM<sub>2.5</sub> concentrations.

409 However, during late spring and fall periods, the correlation between PM<sub>2.5</sub> and O<sub>3</sub>  
410 concentrations was positive compared to the negative in winter. This result suggests  
411 that during heavy aerosol condition (the solar radiation was depressed), the O<sub>3</sub>  
412 chemical production was still high, appearing a double peak of PM<sub>2.5</sub> and O<sub>3</sub> during  
413 fall period. This co-occurrence of high PM<sub>2.5</sub> and O<sub>3</sub> is the focus of this study. The  
414 results are highlighted as follows;

415

416 (1) There are high daytime HONO concentrations in major Chinese mega cities, such  
417 as in Beijing and Shanghai. It is also interesting to note that the high HONO  
418 concentrations were occurred during high aerosol concentration periods. Under  
419 the high daytime HONO concentrations, HONO can be photo-dissociated to be  
420 OH radicals, and becomes an important process to produce OH.

421 (2) With including the OH production of measured HONO concentrations, the  
422 calculated OH concentrations are significantly higher than without including this  
423 production. For example, without HONO production, the maximum OH  
424 concentration is about  $7.5 \times 10^5 \text{#/cm}^3$  under low aerosol condition (AOD=0.25),  
425 and rapidly reduced to  $1.5 \times 10^5 \text{#/cm}^3$  under high aerosol condition (AOD=2.5) in  
426 September. In contrast, by including HONO production, the OH concentrations  
427 significantly increased. For example, under higher aerosol condition (AOD=2.5),  
428 the maximum of OH concentration is about  $7.5 \times 10^5 \text{#/cm}^3$ , which is similar to the  
429 value under low aerosol condition in the no-HONO case. This result suggests that  
430 even under the high aerosol conditions, the chemical oxidizing process for O<sub>3</sub>  
431 production can be active. This result is likely for explaining the co-occurrence of  
432 high PM<sub>2.5</sub> and high O<sub>3</sub> in fall season in eastern China.

433 (3) The measurement of O<sub>3</sub> also shows that the concentrations in winter were always  
434 low, suggesting that the O<sub>3</sub> concentrations were not significantly affected by the  
435 appearance of HONO. The calculated result shows that the seasonal variation of  
436 solar radiation plays important roles for controlling the OH production in winter.  
437 Because the solar radiation is in a very low level in winter, adding the photolysis  
438 of HONO has smaller effect in winter than in fall, and OH remains low values by  
439 including the HONO production term.

440 Because in recent years, the PM<sub>2.5</sub> pollutions are reduced due to the large control  
441 efforts by the Chinese government, the O<sub>3</sub> pollutions become another severe pollution  
442 problem in eastern China. This study is important, because it provides some important

443 scientific highlights to better understand the O<sub>3</sub> pollutions in eastern China.

444

445 **Data availability.** The data used in this paper can be provided upon request from  
446 Xuexi Tie (tiexx@ieecas.cn).

447

448 **Author contributions.** XT came up with the original idea of investigating the  
449 scientific issue. XT and JX designed the analysis method. XL, GL and SZ provided  
450 the observational data and helped in discussion. XT prepared the manuscript with  
451 contributions from all co-authors.

452

#### 453 **Acknowledgement**

454 This work was supported by the National Natural Science Foundation of China  
455 (NSFC) under Grant Nos. 41430424 and 41730108. The Authors thanks the supports  
456 of Center for Excellence in Urban Atmospheric Environment, Institute of Urban  
457 Environment, Chinese Academy of Sciences.

458

459

460      **References**

461

462      Bian H., S.Q. Han, X. Tie, M.L. Shun, and A.X. Liu, Evidence of Impact of Aerosols  
463      on Surface Ozone Concentration: A Case Study in Tianjin, China, *Atmos.*  
464      *Environ.*, 41, 4672-4681, 2007.

465      Chameides, W. L., Fehsenfeld, F., Rodgers, M. O., Cardelino, C., Martines, J., Parrish,  
466      D., Lonneman, W., Lawson, D. R., Ras- mussen, R. A., Zimmerman, P.,  
467      Greenberg, J., Middleton, P., and Wang, T.: Ozone precursor relationships in the  
468      ambient atmo- sphere, *J. Geophys. Res.*, 97, 6037–6055, 1992.

469      Deng X.J, X Tie, D. Wu, XJ Zhou, HB Tan, F. Li, C. Jiang, Long-term trend of  
470      visibility and its characterizations in the Pearl River Delta Region (PRD), China,  
471      *Atmos. Environ.*, 42, 1424-1435, 2008.

472

473      Geng, F.H., C.S., Zhao, X. Tang, GL. Lu, and X. Tie, Analysis of ozone and VOCs  
474      measured in Shanghai: A case study, *Atmos. Environ.*, 41, 989-1001, 2007.

475      Geng, FH, CG Cai, X. Tie, Q. Yu, JL An, L. Peng, GQ Zhou, JM Xu, Analysis of  
476      VOC emissions using PCA/APCS receptor model at city of Shanghai, China, *J.*  
477      *Atmos. Chem.*, 62, 229–247, DOI :10.1007/s10874-010-9150-5, 2010.

478

479      He, S., & Carmichael, G. R. (1999). Sensitivity of photolysis rates and ozone pro-  
480      duction in the troposphere to aerosol properties. *Journal of Geophysical Research: Atmospheres*, 104(D21), 26307-26324.

481

482      Huang, J.P, X. Y. Liu, C. Y. Li, L. Ding, H. P. Yu, The global oxygen budget and its  
483      future projection. *Science Bull.* 63, 1180–1186, 2018.

484

485      Huang J., Y. Li, C. Fu, F. Chen, Q. Fu, A. Dai, M. Shinoda, Z. Ma, W. Guo, Z. Li, L.  
486      Zhang, Y. Liu, H. Yu, Y. He, Y. Xie, X. Guan , M. Ji, L. Lin, S. Wang, H. Yan  
487      and G. Wang, Dryland climate change recent progress and challenges. *Rev. of*  
488      *Geophys.*, 55, 719-778, doi:10.1002/2016RG000550, 2017.

489

490      Huang, R. J., L. Yang, JJ Cao, QY Wang, X. Tie, et al., Concentration and sources of  
491      atmospheric nitrous acid (HONO) at an urban site in Western China. *Sci. of Total*  
492      *Environ.*, 593-594, 165-172, doi.org/10.1016/j.scitotenv.2017.02.166, 2017.

493      Lei, W., R. Zhang, X. Tie, P. Hess, Chemical characterization of ozone formation in  
494      the Houston-Galveston area, *J. Geophys. Res.*, 109, doi:10.1029/2003JD004219,  
495      2004.

496      Li, G., Bei, N., Cao, J., Wu, J., Long, X., Feng, T., Dai, W., Liu, S., Zhang, Q., and  
497      Tie, X.: Widespread and persistent ozone pollution in eastern China during the  
498      non-winter season of 2015: observations and source attributions, *Atmos. Chem.*  
499      *Phys.*, 17, 2759-2774, doi:10.5194/acp-17-2759-2017, 2017.

500      Long, X., X. Tie, JJ Cao, RJ Huang, T. Feng, N. Li, SY Zhao, J. Tian, GH Li, Q.  
501      Zhang, Impact of crop field burning and mountains on heavy haze in the North  
502      China Plain: A case study, *Atmos. Chem. Phys.*, 16, 9675-9691,

503 doi:10.5194/acp-16-9675-2016, 2016.

504 505 Madronich, S. & Flocke, S. in *Environmental Photochemistry 2 / 2L*, 1–26 (Springer Berlin Heidelberg, 1999)

506 507 508 509 Quan, J.N., Y. Gao, Q. Zhang, X. Tie\*, JJ Cao, SQ Han, JW Meng, PF Chen, DL Zhao, Evolution of Planetary Boundary Layer under different weather conditions, and its impact on aerosol concentrations, *Particuology*, doi: 10.1016/j.partic.2012.04.005, 2013.

510 511 Seinfeld, J. H. and Pandis, S. N.: *Atmospheric Chemistry and Physics: From Air Pollution to Climate Change*, 2nd Edn., John Wiley and Sons, New York, 2006.

512 513 514 Shi, C., Wang, S., Liu, R., Zhou, R., Li, D., Wang, W., ... & Zhou, B. (2015). A study of aerosol optical properties during ozone pollution episodes in 2013 over Shanghai, China. *Atmospheric Research*, 153, 235-249.

515 516 517 Sillman, S.: The use of NO<sub>y</sub>, H<sub>2</sub>O<sub>2</sub>, and HNO<sub>3</sub> as indicators for ozone-NO<sub>x</sub>-hydrocarbon sensitivity in urban locations, *J. Geo- phys. Res.*, 100, 14175–14188, 1995.

518 519 520 Tie, X., G. Brasseur, C. Zhao, C. Granier, S. Massie, Y. Qin, P.C. Wang, GL Wang, PC, Yang100,, Chemical Characterization of Air Pollution in Eastern China and the Eastern United States, *Atmos. Environ.*, 40. 2607-2625, 2006.

521 Tie, X., D. Wu, and G. Brasseur, Lung Cancer Mortality and Exposure to Atmospheric Aerosol Particles in Guangzhou, China, *Atmos. Environ.*, 43, 2375–2377, 2009a.

525 526 527 Tie, X., FH. Geng. L. Peng, W. Gao, and CS. Zhao, Measurement and modeling of O<sub>3</sub> variability in Shanghai, China; Application of the WRF-Chem model, *Atmos. Environ.*, 43, 4289-4302, 2009b.

528 529 530 531 532 Tie X., F. Geng, A. Guenther, J. Cao, J. Greenberg, R. Zhang, E. Apel, G. Li, A. Weinheimer, J. Chen, and C. Cai, Megacity impacts on regional ozone formation: observations and WRF-Chem modeling for the MIRAGE-Shanghai field campaign, *Atmos. Chem. Phys.*, 13, 5655-5669, doi:10.5194/acp-13-5655-2013, 2013.

533 534 Tie, X., Q. Zhang, H. He, JJ Cao, SQ Han, Y. Gao, X. Li, and XC Jia, A budget analysis on the formation of haze in Beijing, *Atmos. Environ.*, 25-36, 2015.

535 536 537 Tie, X., RJ Huang, WT Dai, JJ Cao, X. Long, XL Su, SY Zhao, QY Wang, GH Li, Effect of heavy haze and aerosol pollution on rice and wheat productions in China, *Sci. Rep.* 6, 29612; doi: 10.1038/srep29612, 2016.

538 539 Tie, X., J.J. Cao, Understanding Variability of Haze in Eastern China, *J Fundam Renewable Energy Appl*, 7:6 DOI: 10.4172/2090-4541.100024, 2017.

540 Tie, X., R.J. Huang, J.J. Cao, Q. Zhang, Y.F. Cheng, H. Su, D. Chang, U. Pöschl, T.

541 Hoffmann, U. Dusek, G. H. Li, D. R. Worsnop, C. D. O'Dowd, Severe Pollution  
542 in China Amplified by Atmospheric Moisture, *Sci. Rep.* 7: 15760 |  
543 DOI:10.1038/s41598-017-15909-1, 2017.

544 Zhang, L., Wang, T., Zhang, Q., Zheng, J., Xu, Z., & Lv, M.. Potential sources of  
545 nitrous acid (HONO) and their impacts on ozone: A WRF/Chem study in a  
546 polluted subtropical region. *Journal of Geophysical Research: Atmospheres*,  
547 121(7), 3645- 3662, 2016.

548 Zhang, R., X. Tie, and D. Bond, Impacts of Anthropogenic and Natural NO<sub>x</sub> Sources  
549 over the U.S. on Tropospheric Chemistry, *Proceedings of National Academic  
550 Science USA*, 100, 1505-1509, 2003.

552 Zhang, Q., C. Zhao, X. Tie, Q. Wei ,G. Li, and C. Li, Characterizations of Aerosols  
553 over the Beijing Region: A Case Study of Aircraft Measurements, 40,  
554 4513-4527, *Atmos. Environ.*, 2006.

555

556

557 **Figure Caption**  
558

559 **Fig. 1.** The geographic locations of the measurement sites in Beijing, in which the  
560 measured concentrations of  $\text{PM}_{2.5}$  and  $\text{O}_3$  are used to the analysis.

561 **Fig. 2.** The daily averaged concentrations of  $\text{PM}_{2.5}$  and  $\text{O}_3$  in the Beijing region in  
562 2015. The concentrations are averaged over all sites shown in Fig. 1. The blue lines  
563 represent the  $\text{PM}_{2.5}$  concentrations ( $\mu\text{g}/\text{m}^3$ ), and the red bars represent the  $\text{O}_3$   
564 concentrations ( $\mu\text{g}/\text{m}^3$ ). The rectangles show some typical events during winter  
565 (green), spring and fall (orange), and summer (red).

566 **Fig. 3.** The correlation between  $\text{O}_3$  and  $\text{PM}_{2.5}$  concentrations during winter (upper  
567 panel) and during late spring and fall (lower panel). During winter,  $\text{O}_3$  concentrations  
568 were strong anti-correlated with the  $\text{PM}_{2.5}$  concentrations. During late spring and fall,  
569  $\text{O}_3$  concentrations were correlated with the  $\text{PM}_{2.5}$  concentrations.

570 **Fig. 4.** The diurnal variations of  $\text{PM}_{2.5}$  (blue line) and  $\text{O}_3$  (red line), and  $\text{NO}_2$  (green  
571 line) during a fall period (from Oct. 5 to Oct. 6, 2015). It shows that with high  $\text{PM}_{2.5}$   
572 condition, there was a strong  $\text{O}_3$  diurnal variation.

573 **Fig. 5.** The cloud condition during the period of the case study (between Oct 5 and 6,  
574 2015) in the Beijing region. The bright white color shows the cloud covers, and the  
575 grey white shows the haze covers. The Beijing region was under the heavy haze  
576 conditions during the period.

577 **Fig. 6.** The measured solar radiation ( $\text{W}/\text{m}^2$ ) from Oct. 3 to Oct. 9, 2015 in Beijing.  
578 The upper panel shows hourly values, and the lower panel shows the daytime  
579 averaged values.

580 **Fig. 7.** The effect of aerosol levels with  $\text{AOD} = 0.25$  (black line),  $\text{AOD} = 2.5$  (red  
581 line),  $\text{AOD} = 3.5$  (blue line), and  $\text{AOD} = 4.0$  (green line) on the  $\text{O}_3$  photolysis  
582 calculated by the TUV model in October at middle-latitude.

583 **Fig. 8.** The measured  $\text{HONO}$  concentrations (ppbv) in three large cities in China. The  
584 red line was measured in Xi'An from 24 July to August 6, 2015. The blue line was  
585 measured in Shanghai from 9 to 18 September, 2009. The dark-red line was measured  
586 in Beijing from 1 to 27 January, 2014. The green line is calculated by the WRF-Chem  
587 model. The measurement in fall of Shanghai is applied to the calculation for the OH  
588 production of  $\text{HONO}$ .

589 **Fig. 9.** The measured  $\text{HONO}$  (upper panel) and  $\text{PM}_{2.5}$  concentrations (lower panel) in  
590 fall in Shanghai. It illustrates that the high  $\text{HONO}$  concentrations were corresponded  
591 with high  $\text{PM}_{2.5}$  concentrations.

592 **Fig. 10.** The calculated OH production  $P(\text{HOx})$  ( $\#/ \text{cm}^3/\text{s}$ ) by using the model  
593 calculated  $\text{HONO}$  (low concentrations) (in the upper panel) and by using the  
594 measured  $\text{HONO}$  (high concentrations) (in the lower panel). The red bars represent  
595 the calculation of the P1 term, and the red bars represent the calculation of the P2  
596 term (OH production from  $\text{HONO}$ ).

607 **Fig. 11.** The calculated OH concentrations (#/cm<sup>3</sup>) with (upper panel) and without  
608 (lower panel) HONO production of OH, under different aerosol levels. Dark red  
609 (AOD=0.25), red (AOD=2.5) ), red (AOD=3.5) ), and red (AOD=4.0).

610

611 **Fig. 12.** The effect of cloud cover on the photolysis rate of HONO (J[HONO]). The  
612 blue, red, and green lines represent the cloud water vapor of 0 (cloud-free), 10 (g/m<sup>3</sup> –  
613 thin cloud), and 50 (g/m<sup>3</sup> – thick cloud), respectively. The left panel (A) represents  
614 the light aerosol condition, with AOD of 0.25, and the right panel (B) represents the  
615 heavy aerosol condition, with AOD of 2.5.

616

617 **Fig. 13.** The calculated OH concentrations in September (blue bars) and December  
618 (dark red bars), under different aerosol levels.

619

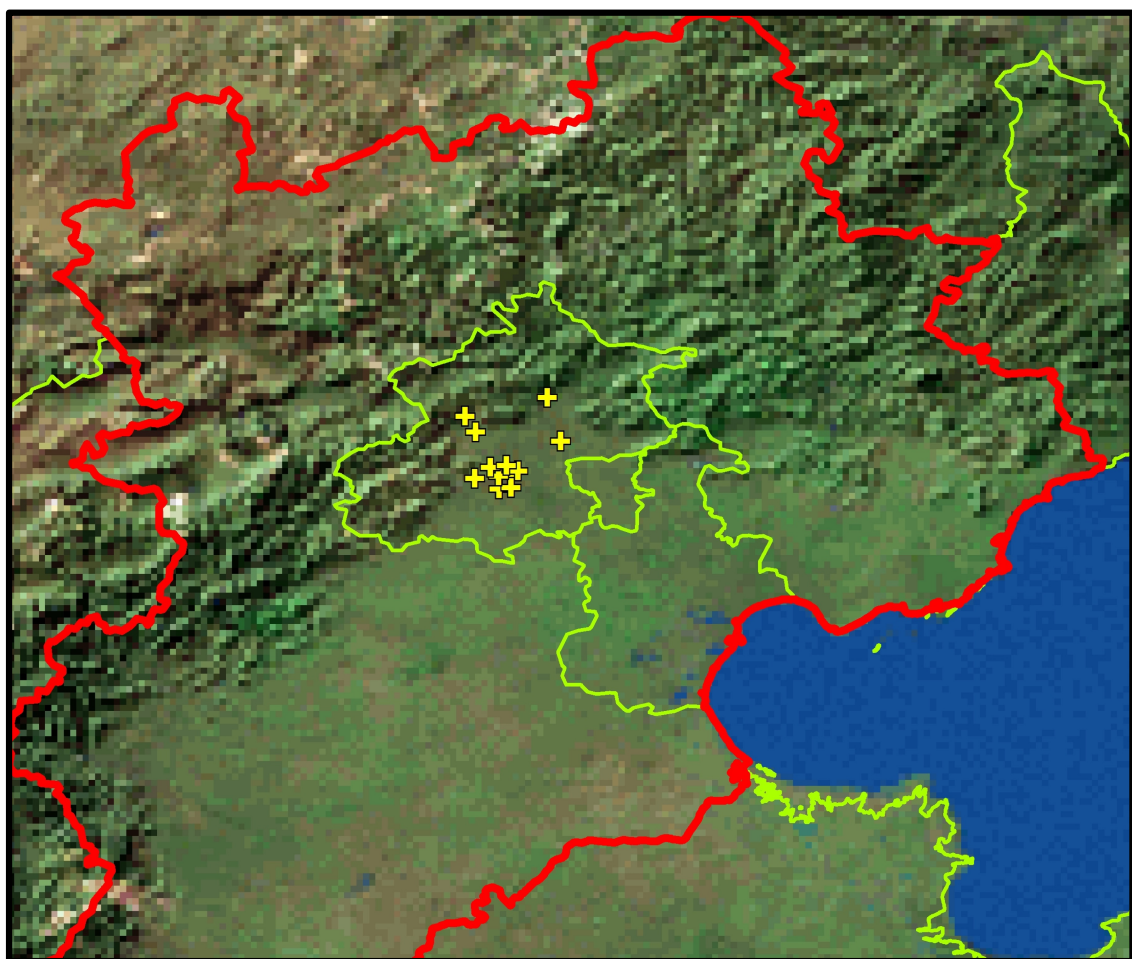
620

621

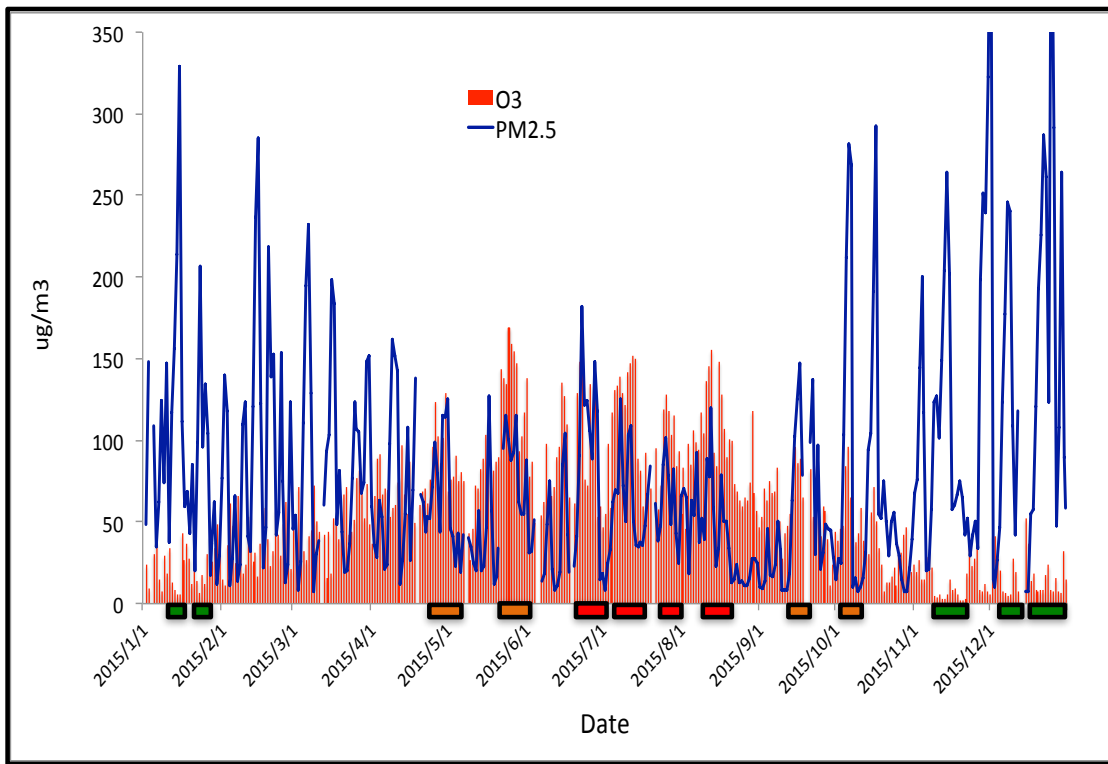
622

623  
624

## Figures

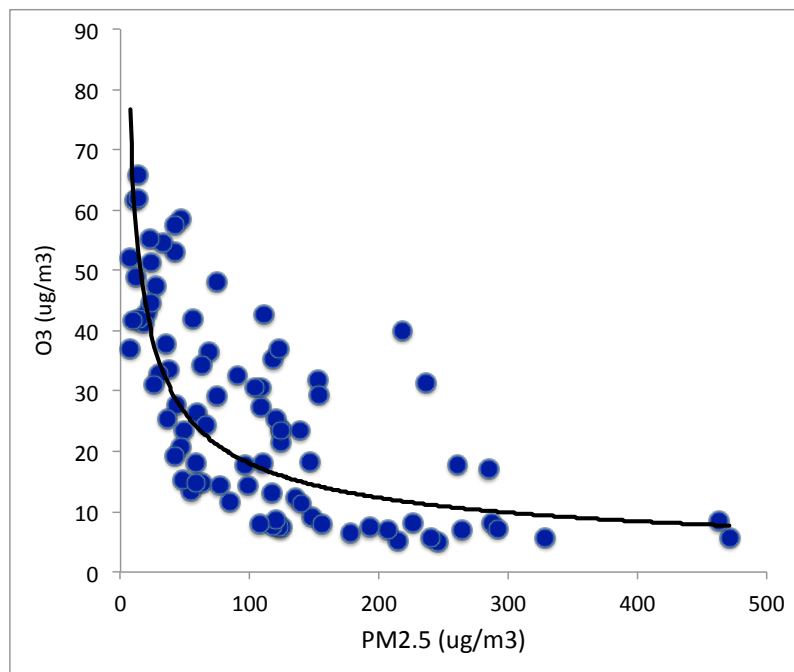


625  
626  
627 **Fig. 1.** The geographic locations of the measurement sites in Beijing, in which the measured  
628 concentrations of  $PM_{2.5}$  and  $O_3$  are used to the analysis.  
629



630  
631  
632  
633  
634  
635  
636  
637  
638  
639  
640

**Fig. 2.** The daily averaged concentrations of PM<sub>2.5</sub> and O<sub>3</sub> in the Beijing region in 2015. The concentrations are averaged over all sites shown in Fig. 1. The blue lines represent the PM<sub>2.5</sub> concentrations ( $\mu\text{g}/\text{m}^3$ ), and the red bars represent the O<sub>3</sub> concentrations ( $\mu\text{g}/\text{m}^3$ ). The rectangles show some typical events during winter (green), spring and fall (orange), and summer (red).



641  
642

643  
644  
645  
646  
647  
648  
649  
650

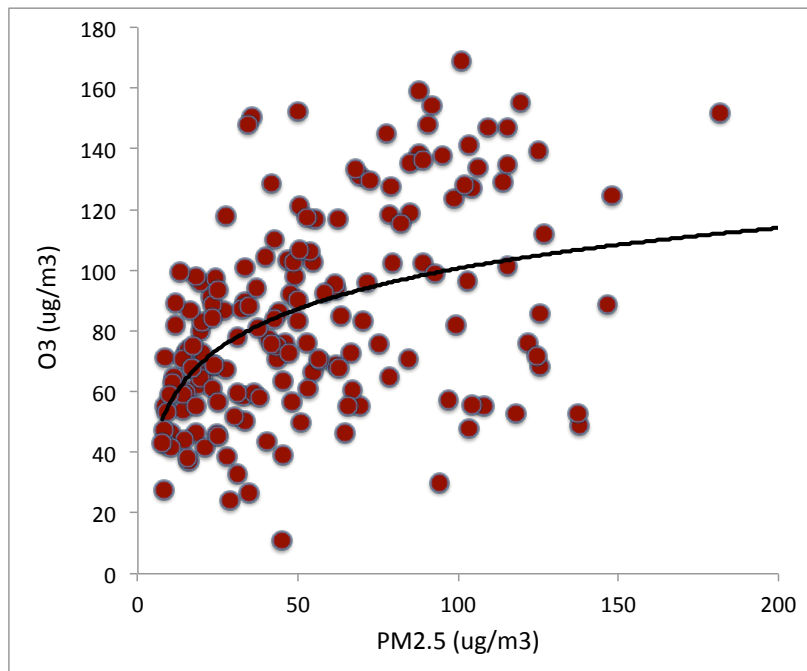


**Fig. 3.** The correlation between  $O_3$  and  $PM_{2.5}$  concentrations during winter (upper panel) and during late spring and fall (lower panel). During winter,  $O_3$  concentrations were strong anti-correlated with the  $PM_{2.5}$  concentrations. During late spring and fall,  $O_3$  concentrations were correlated with the  $PM_{2.5}$  concentrations.

651  
652  
653  
654  
655  
656  
657

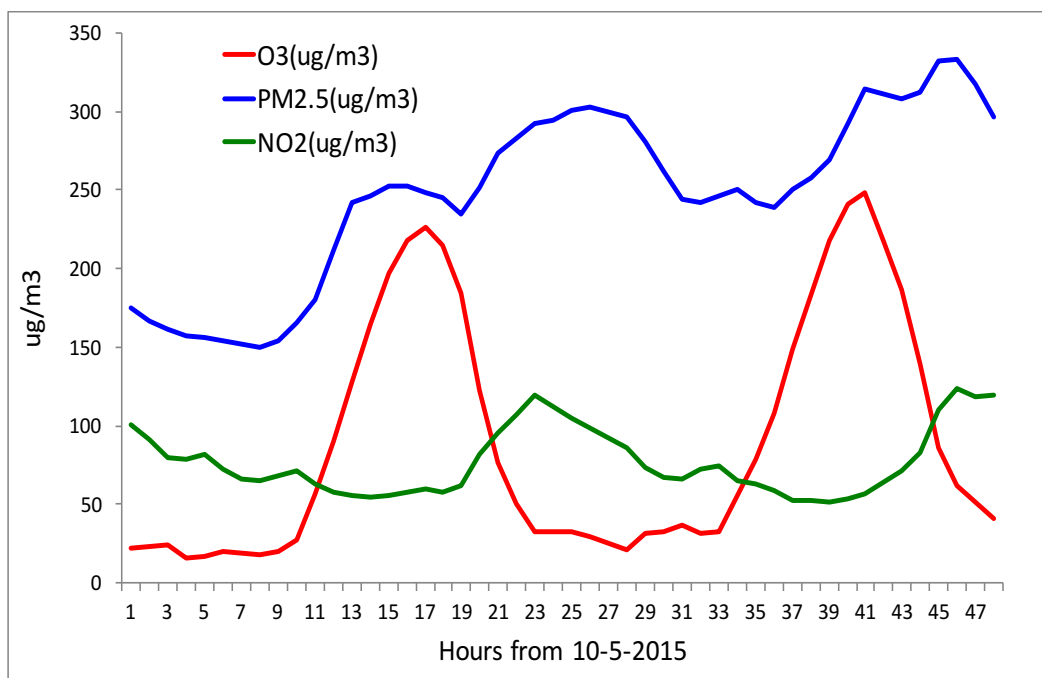
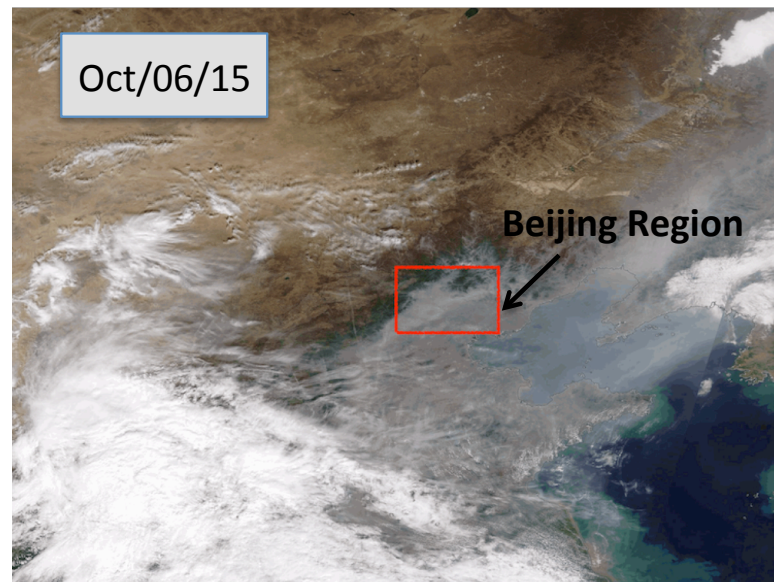
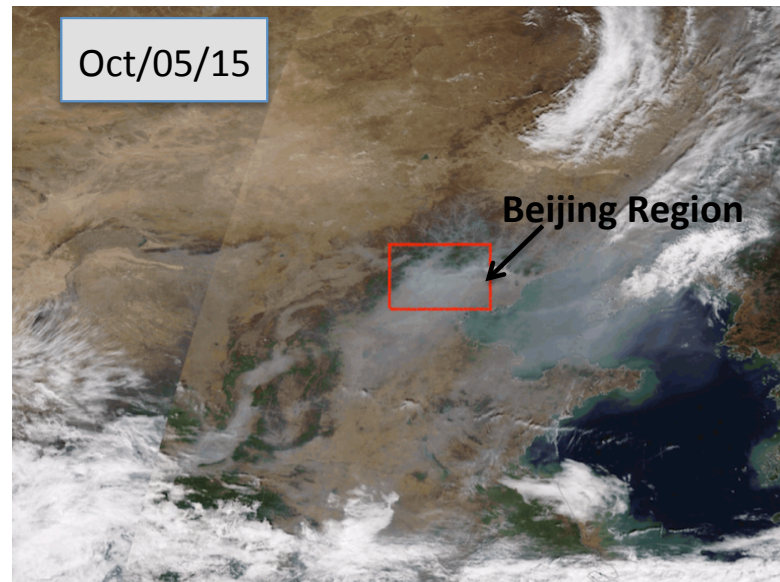
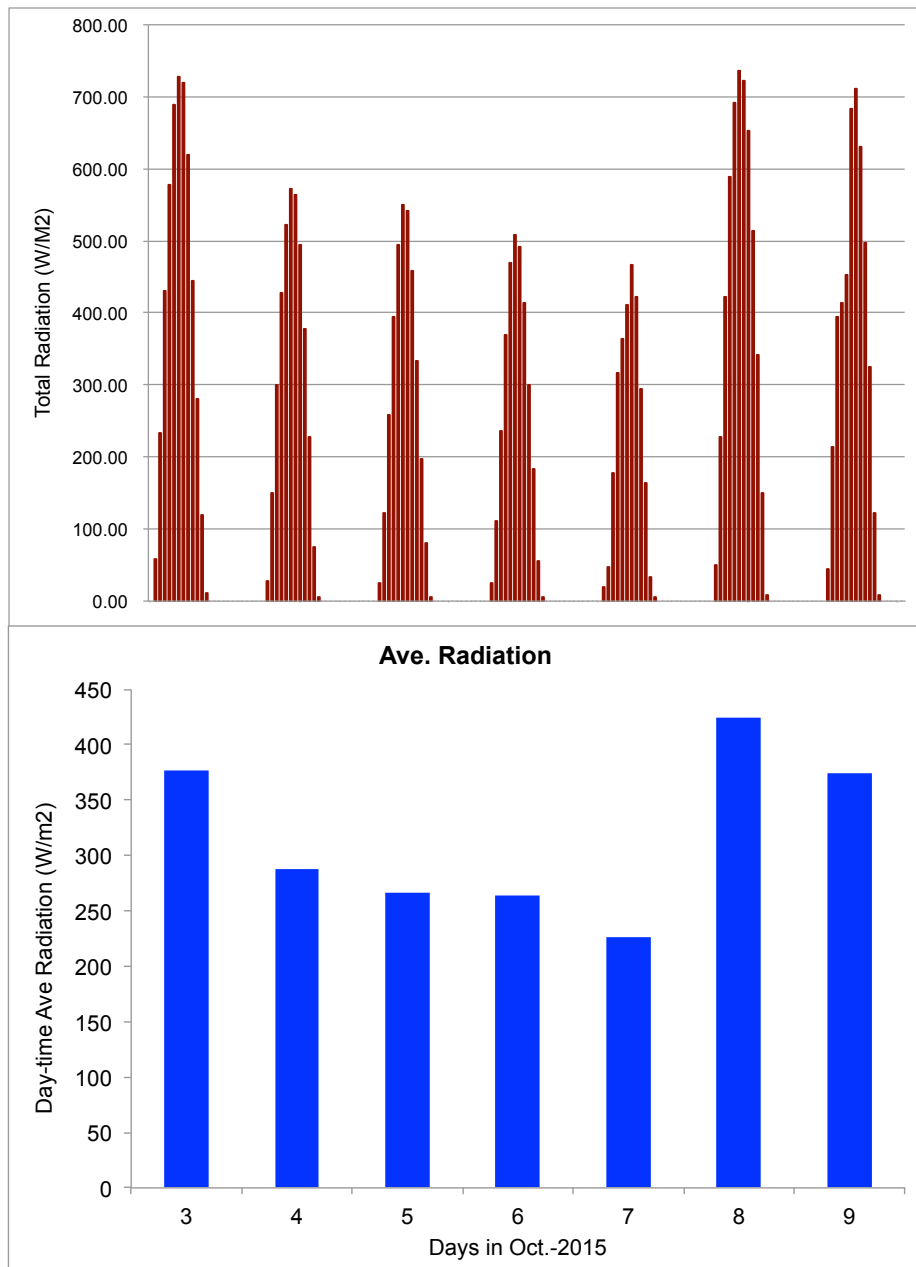


**Fig. 4.** The diurnal variations of  $PM_{2.5}$  (blue line) and  $O_3$  (red line), and  $NO_2$  (green line) during a fall period (from Oct. 5 to Oct. 6, 2015). It shows that with high  $PM_{2.5}$  condition, there was a strong  $O_3$  diurnal variation.



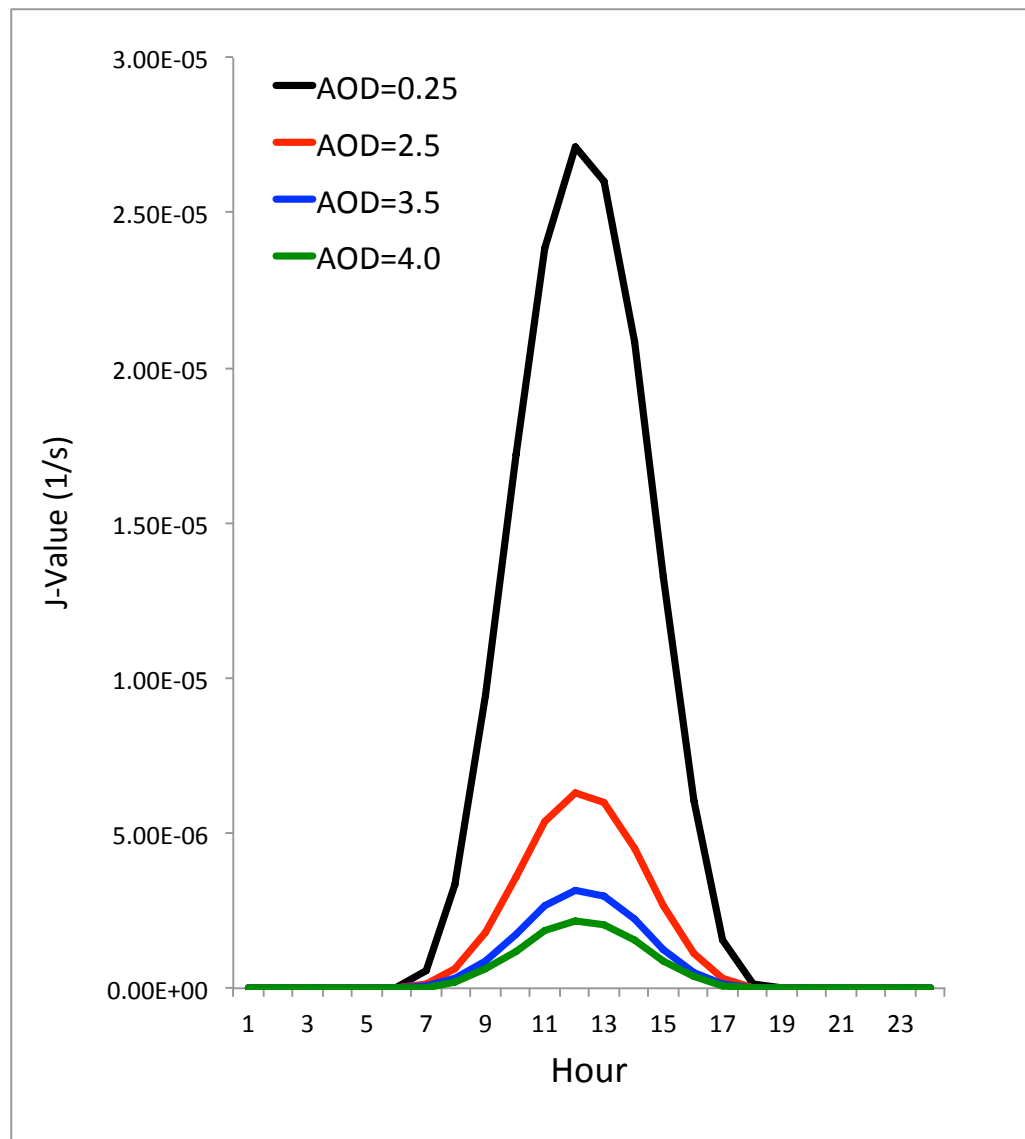
658  
659  
660  
661  
662

**Fig. 5.** The cloud condition during the period of the case study (between Oct 5 and 6, 2015 in the Beijing region. The bright white color shows the cloud covers, and the grey white shows the haze covers. The Beijing region is under the heavy haze conditions during the period.



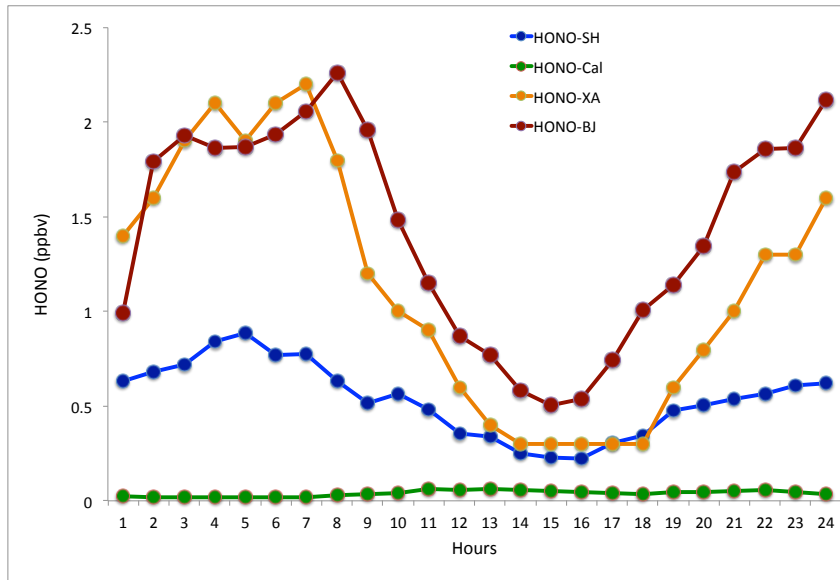
663  
664  
665  
666  
667

**Fig. 6.** The measured solar radiation ( $\text{W/m}^2$ ) from Oct. 3 to Oct. 9, 2015 in Beijing. The upper panel shows hourly values, and the lower panel shows the daytime averaged values.



668  
669  
670  
671  
672  
673

**Fig. 7.** The effect of aerosol levels with AOD = 0.25 (black line), AOD = 2.5 (red line), AOD = 3.5 (blue line), and AOD = 4.0 (green line) on the  $\text{O}_3$  photolysis calculated by the TUV model in October at middle-latitude.



674  
675  
676  
677 **Fig. 8.** The measured HONO concentrations (ppbv) in three large cities in China.  
678 The red line was measured in Xi'An from 24 July to August 6, 2015. The blue line  
679 was measured in Shanghai from 9 to 18 September, 2009. The dark-red line was  
680 measured in Beijing from 1 to 27 January, 2014. The green line is calculated by the  
681 WRF-Chem model. The measurement in fall of Shanghai is applied to the  
682 calculation for the OH production of HONO.  
683

684  
685  
686  
687  
688

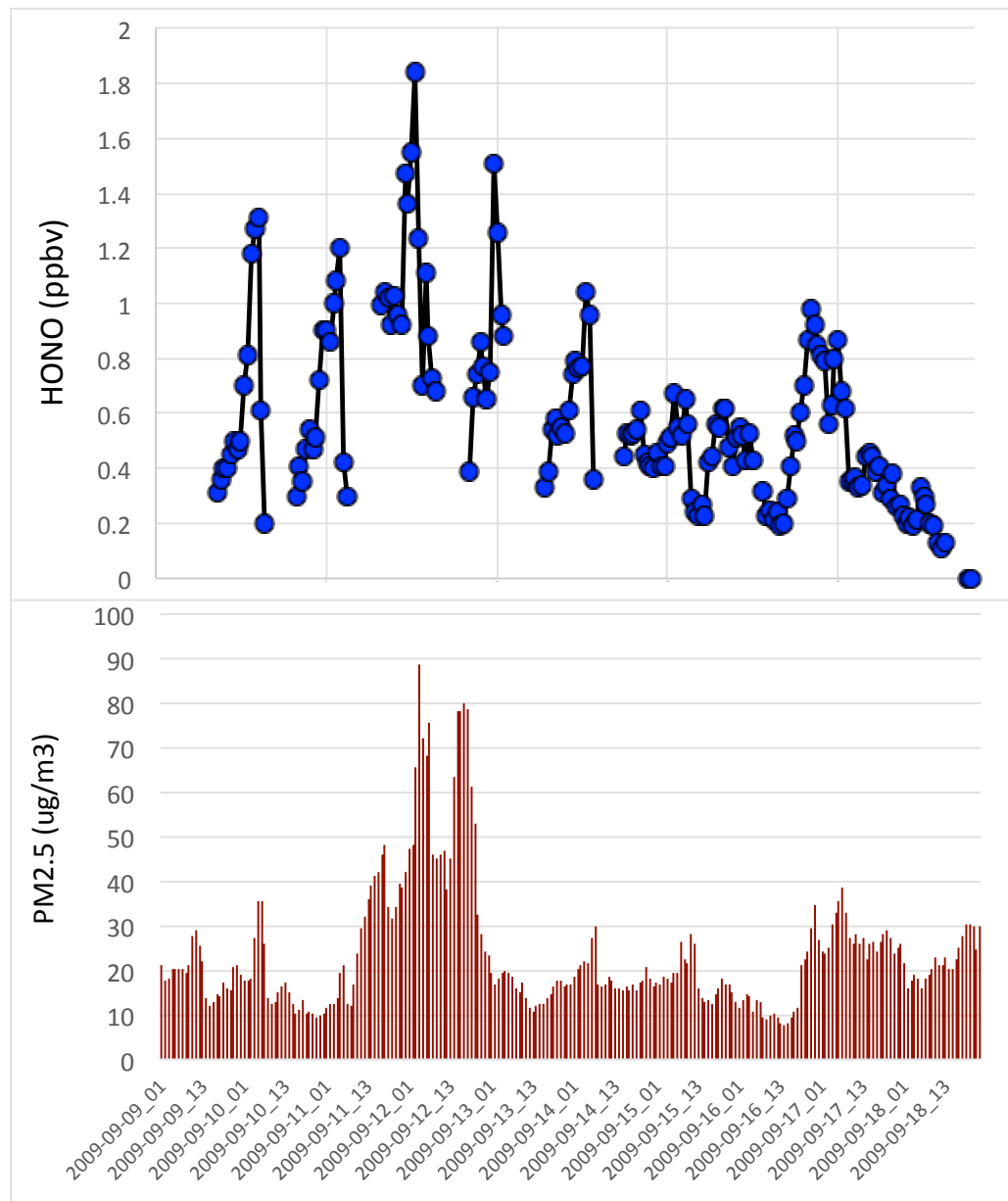
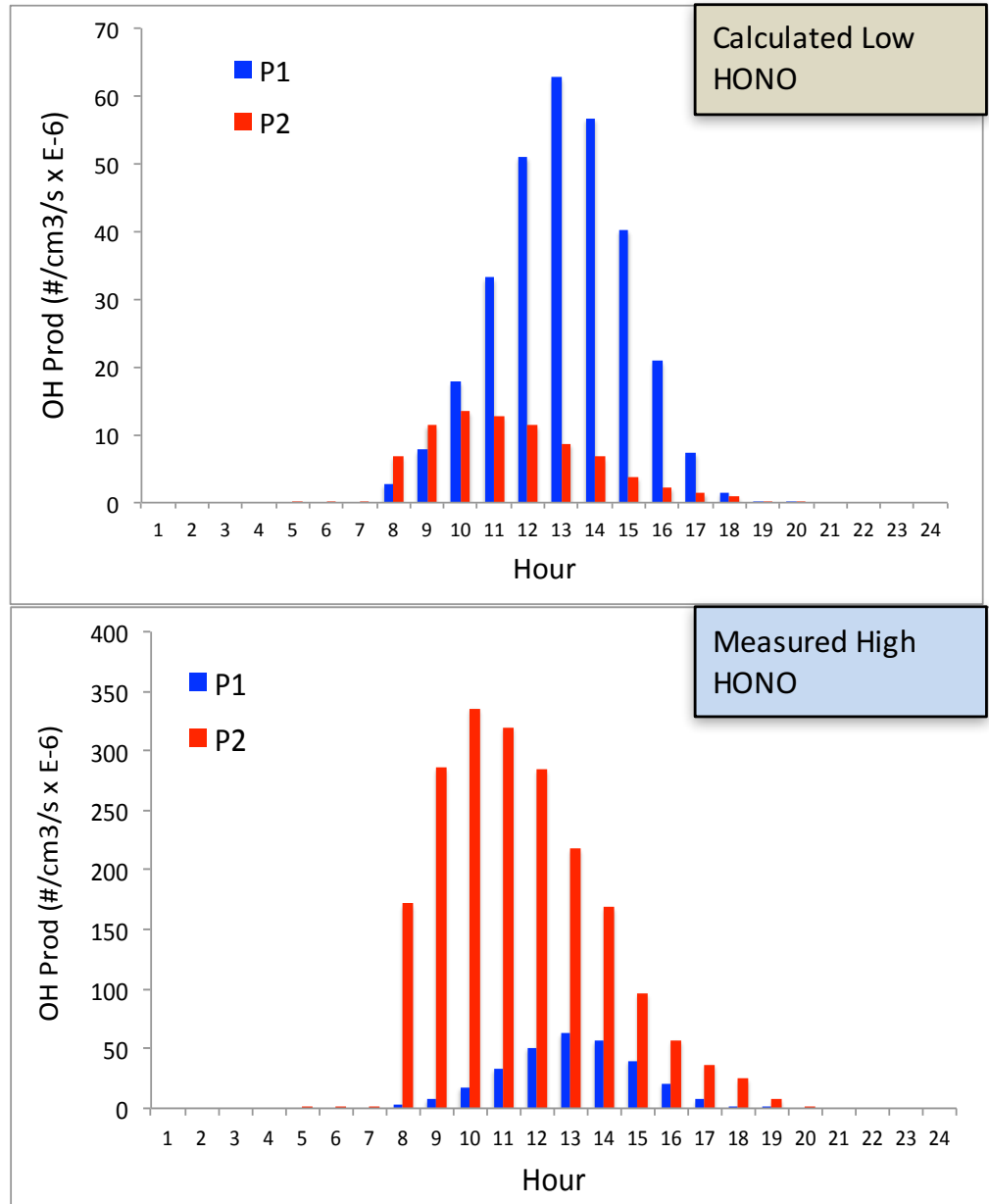
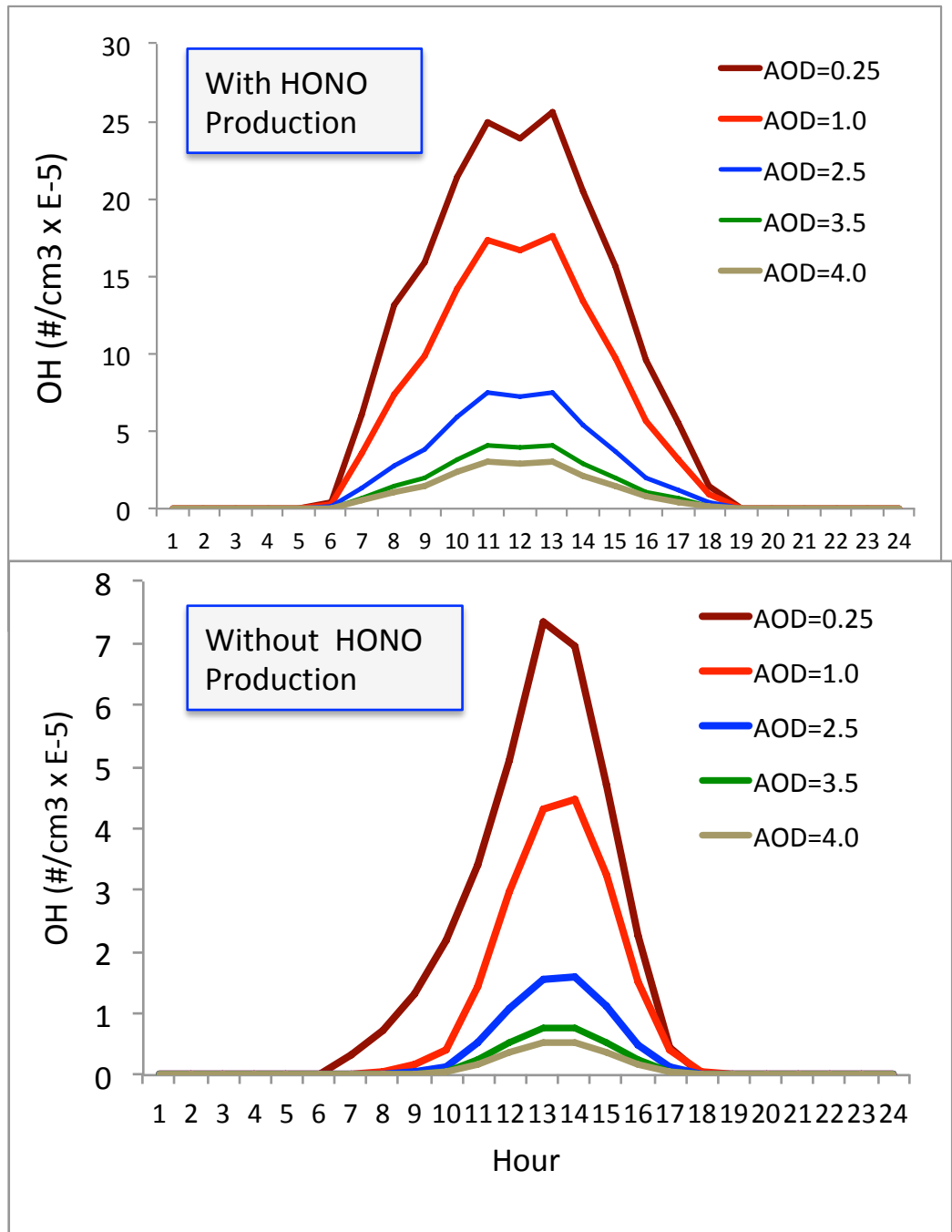


**Fig. 9.** The measured HONO (upper panel) and PM<sub>2.5</sub> concentrations (lower panel) in fall in Shanghai. It illustrates that the high HONO concentrations were corresponded with high PM<sub>2.5</sub> concentrations.



689  
690  
691 Fig. 10. The calculated OH production  $P(HOx)$  ( $\#/cm^3/s$ ) by using the model calculated  
692 HONO (low concentrations) (in the upper panel) and by using the measured HONO  
693 (high concentrations) (in the lower panel). The red bars represent the calculation of the  
694 P1 term, and the red bars represent the calculation of the P2 term (OH production from  
695 HONO).



696  
697  
698  
699  
700  
701  
702  
703  
**Fig. 11.** The calculated OH concentrations ( $\#/cm^3$ ) with (upper panel) and without (lower panel) HONO production of OH, under different aerosol levels. Dark red (AOD=0.25), red (AOD=2.5), red (AOD=3.5), and red (AOD=4.0).

704  
705  
706  
707  
708  
709  
710  
711  
712  
713  
714  
715

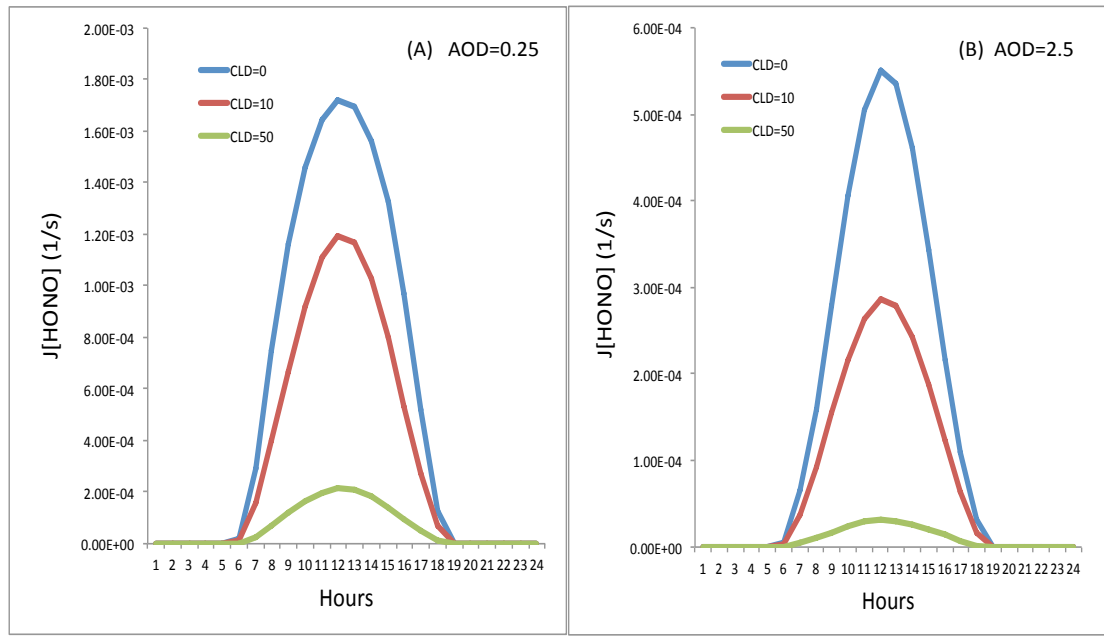
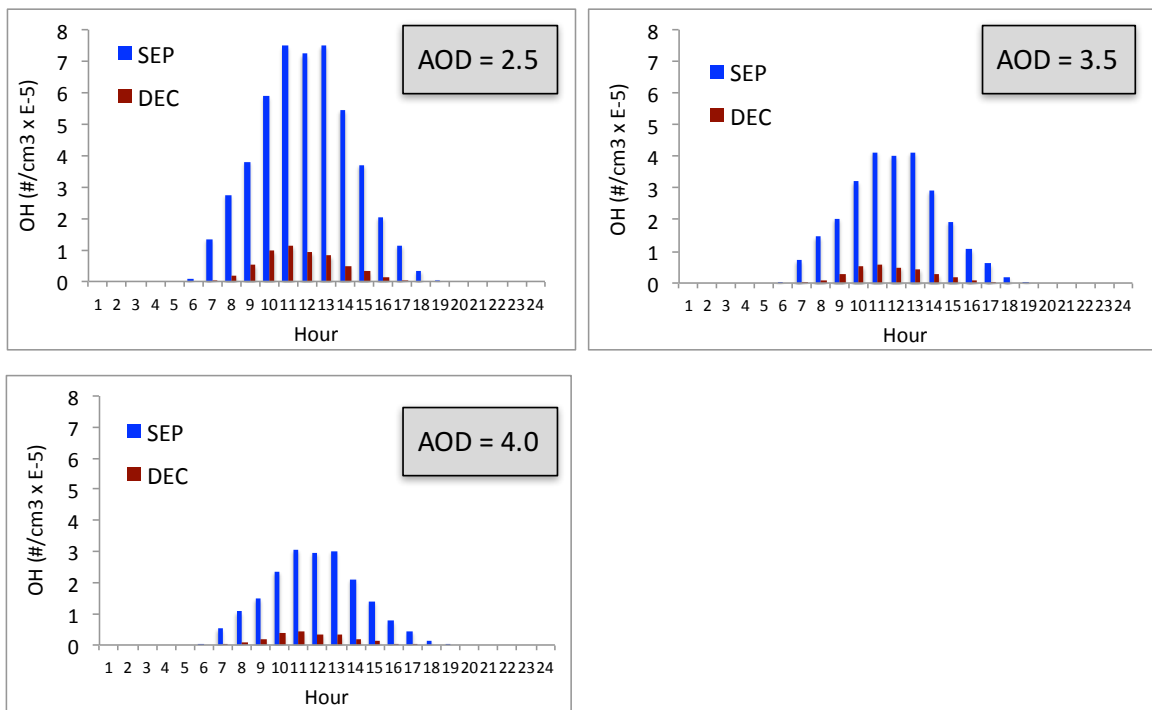


**Fig. 12.** The effect of cloud cover on the photolysis rate of HONO ( $J[HONO]$ ). The blue, red, and green lines represent the cloud water vapor of 0 (cloud-free), 10 ( $g/m^3$  – thin cloud), and 50 ( $g/m^3$  – thick cloud), respectively. The left panel (A) represents the light aerosol condition, with AOD of 0.25, and the right panel (B) represents the heavy aerosol condition, with AOD of 2.5.

716  
717



718  
719  
720  
721  
722

**Fig. 13.** The calculated OH concentrations in September (blue bars) and December (dark red bars), under different aerosol levels.